Environmental Science and Pollution Research (2020) 27:40826–40836
https://doi.org/10.1007/s11356-020-10120-8

RESEARCH ARTICLE

Simultaneous removal of chromium(VI) and tetracycline hydrochloride from simulated wastewater by nanoscale zero-valent iron/copper–activated persulfate

Guangzhou Qu[1,2] · Rongjie Chu[1] · Hui Wang[1] · Tiecheng Wang[1,2] · Zengqiang Zhang[1,2] · Hong Qiang[1,2] · Dongli Liang[1,2] · Shibin Hu[1,2]

Received: 9 December 2019 / Accepted: 13 July 2020 / Published online: 16 July 2020

Abstract

In this paper, metallic copper (Cu) was supported on nanoscale zero-valent iron (nZVI) to form a nanoscale bimetallic composite (nZVI-Cu), which was used to activate persulfate (PS) to simultaneously remove the compound contaminants Cr(VI) and tetracycline hydrochloride (TCH) in simulated wastewater. nZVI, nZVI-Cu, and nZVI-Cu-activated PS (nZVI-Cu/PS) were characterized by SEM, TEM, XRD, and XPS. The effects of the bimetallic composite on Cr(VI) and TCH removal were compared in the nZVI, nZVI-activated PS (nZVI/PS), nZVI-Cu, and nZVI-Cu/PS systems. The results showed that nZVI and Cu can form a nanobimetallic system, which can create galvanic cells; thus, the galvanic corrosion of nZVI and the transfer of electrons are accelerated. For a single contaminant, the removal efficiency of Cr(VI) and TCH is the highest when nZVI is loaded with 3 wt% and 1 wt% Cu, respectively. The ratio of nZVI-Cu with 3 wt% Cu to PS is 7:1, and the removal efficiency of Cr(VI) and TCH compound contaminants is ~ 100% after 60 min under acidic conditions, which indicates that the Cr(VI) reduction and TCH oxidation were complete in the nZVI-Cu/PS system. The mechanisms of simultaneous removal of Cr(VI) and TCH in the nZVI-Cu/PS system are proposed. The removal of Cr is because of the adsorption-reduction effects of the nZVI-Cu bimetallic material. The degradation of TCH is mainly due to the action of oxidative free radicals generated by Fe^{2+}-activated PS. The free radical capture experiments showed that SO- 4· plays a major role in the process of TCH degradation.

Keywords Nanoscale zero-valent iron · Persulfate · Oxidative free radical · Cr(VI) · Tetracycline hydrochloride · Removal mechanisms

Introduction

With continuous economic development, the types and concentrations of pollutants increase in water environments, and various types of discharged sewage exhibit complex characteristics, high concentrations, biodegradation resistance, and high toxicity. Traditional biological treatment technology has difficulty meeting increasingly stringent sewage discharge standards. Advanced oxidation technology (AOP) has become a research hotspot for researchers to address such wastewater, and various new oxidation technologies are emerging (Kang et al. 2018).

Persulfate (PS) is activated to produce the strong sulfate radical (SO- 4·), which is considered to be the most promising AOP for remediating contaminated water and soil. Its redox potential (SO- 4·, E_0 = 2.5–3.1 V) even exceeds that of the highly oxidizing hydroxyl radical (·OH, E_0 = 1.8–2.7 V) (Matzek and Carter 2016), which can theoretically degrade most organic pollutants. The commonly used methods for the activation of PS are mainly heat (Waldemer et al. 2007), ultraviolet light (Lin et al. 2011), transition metal ions (Xu and Li 2012), electron beam radiation (Criquet and Leitner 2011), and ultrasonic treatment (Chen and Su 2012). Among the many activation techniques, transition metal ion activation is

Responsible Editor: Vítor Pais Vilar

✉ Guangzhou Qu
qugz@nwsuaf.edu.cn

[1] College of Natural Resources and Environment, Northwest A&F University, Yangling 712100, Shanxi, People's Republic of China

[2] Key Laboratory of Plant Nutrition and the Agri-environment in Northwest China, Ministry of Agriculture, Yangling 712100, Shanxi, People's Republic of China

the most widely used (Song et al. 2019). Transition metal ion (Fe^{2+})-activated PS is used at normal temperature and pressure, and the operation mode is relatively simple and easy to implement. However, Fe^{2+} reacts with PS extremely quickly, and the reaction is usually completed in a few minutes. To overcome this deficiency, some researchers have used Fe^0 as a source of Fe^{2+}, such as Ghauch et al. (2013), to demonstrate the feasibility of using Fe^0 as a source of Fe^{2+} for activating PS to degrade sulfamethoxazole. Li et al. (2017) explored the role of surface Fe species and the synergistic effect of ·OH and SO-4· on the activation of PS by iron powder.

Nanoscale zero-valent iron (nZVI) is a kind of zero-valent iron particle with a particle size of approximately 1–100 nm. It has high surface energy, magnetic properties, large specific surface area, and excellent adsorption and reaction efficiency for wastewater contaminants. nZVI, as a slow release source of Fe^{2+}, can activate PS to produce SO- 4· to degrade organic compounds (Diao et al. 2016). In addition, adding PS to nZVI was found to improve the efficiency of removing heavy metals by enhancing the corrosion of nZVI (Guo et al. 2016). However, nZVI alone tends to agglomerate to form micron-sized aggregates and forms iron oxides or oxyhydroxides on the surface after reaction, which will result in a decrease in reactivity. To overcome these factors, another active metal, such as Pt, Cu, Ag, and Ni, can be loaded onto the nZVI surface to develop and improve the performance of nZVI. The synthesized bimetallic particles form a microbattery on the nZVI surface to promote electron transfer and accelerate the reaction rate (Wei et al. 2006; Zhu and Lim 2007; Shi et al. 2016; Zeng et al. 2017). Ag and Ni metals have certain toxicity, and Pt is a precious metal and is a relatively expensive synthesis metal for doping. Cu is relatively low cost compared with several precious metals and has low toxicity. The nanoiron-copper bimetal composite prepared by Hosseini et al. (2011) has a suspension time of up to 20 h, a stability that far exceeds that of nanoiron particles, and has higher removal efficiency for target contaminants.

Using metal-modified nZVI to reduce heavy metal adsorption and activated PS to degrade organic pollutants, the two technologies were combined to treat the compound contaminants of heavy metals and organic matter in wastewater. We aimed to elucidate the simultaneous removal mechanisms of heavy metals and organic pollutants involved in PS activation by nZVI-loaded Cu (nZVI-Cu) bimetallic material. The roles of nZVI-Cu on PS activation were studied by investigating the loaded amount of Cu and the ratio of nZVI-Cu to PS in the activation systems. The evolution of the nZVI-Cu core-shell bimetallic structure was analyzed by quantitatively determining the Fe and Cu species during the nZVI-Cu activating PS process. The formation and function of SO- 4· and ·OH were quantitatively predicted by the radical capture experiments.

Experimental

Chemicals and materials

The chemical reagents, including sodium persulfate, tetracycline hydrochloride (TCE), potassium dichromate ($K_2Cr_2O_7$), ethyl alcohol absolute, ferric chloride hexahydrate ($FeCl_3 \cdot 6H_2O$), sodium borohydride ($NaBH_4$), copper nitrate hydrate ($Cu(NO_3)_2 \cdot 3H_2O$), methanol (MA), and tert-butanol (TBA), were analytical reagent grade.

Preparation of nZVI and nZVI-Cu composites

The nZVI was prepared by a chemical reduction method according to that described by Sheng et al. (2014 and 2016). The reaction equation is as follows:

$$4Fe^{3+} + 3BH_4^- + 9H_2O \rightarrow 4Fe_3O_4 + 3H_2BO_3^- + 12H^+ + 6H_2\uparrow \quad (1)$$

In this study, 1.216 g of $FeCl_3 \cdot 6H_2O$ and 1.888 g of $NaBH_4$ were separately dissolved in a 100-mL beaker containing a 3:7 aqueous solution of ethanol and water. Then, $NaBH_4$ was added dropwise to the $FeCl_3$ solution in a 40-kW ultrasonic environment to produce a solid-liquid mixture, which was subjected to solid-liquid separation by a strong magnet to obtain black solid nZVI.

A certain volume of 8.5 mM $Cu(NO_3)_2 \cdot 3H_2O$ solution is slowly dropped into the separated nZVI by the above method. After complete addition and stirring for 15 min, the reaction of Cu^{2+} with Fe^0 was complete. The reaction equation is as follows:

$$Cu^{2+} + Fe^0 \rightarrow Fe^{2+} + Cu^0 \quad (2)$$

After the reaction, the product was washed three times with deoxygenated deionized water and then further washed three times with absolute ethanol to obtain nZVI-Cu bimetallic nanocomposites.

Characterizations

The surface morphology of the nZVI, nZVI-Cu, and nZVI-Cu of activated PS (nZVI-Cu/PS) was characterized by field emission scanning electron microscopy (FESEM, Japanese Hitachi S-4800) and high-resolution transmission electron microscopy (TEM). The crystallization conditions, crystal phase, and crystal structure of the nanomaterial and nZVI-Cu/PS were analyzed using X-ray powder diffraction (XRD, Bruker D8 Advance A25, Germany). The main elemental composition and valence state changes of nZVI and the nZVI-Cu/PS composites were examined using X-ray photoelectron spectroscopy (XPS, Thermo Scientific EscaLab 250Xi, USA).

Experimental procedure

Batch experiments were carried out in a permeable reaction column simulation device made of plexiglass. The experimental device was described in our previous published paper (Qu et al. 2019). The nZVI-Cu bimetal material and PS were simultaneously added to the top of the column, a 500-mL beaker was placed on a magnetic stirrer, and the amount of contaminated wastewater added to the beaker was 400 mL. The simulated wastewater was pumped via a latex tube into the reaction column by a peristaltic pump and then returned to the beaker via the bottom outlet. The process was continuously circulated by a peristaltic pump with a pump flow of about 60 mL/min. The pH value and initial concentrations of Cr(VI) and TCH in solution were 5.0, 40.0, and 100 mg L^{-1}, respectively, unless otherwise stated. Samples were set at different time intervals, and the samples were filtered through a 0.22-mm membrane filter. The concentrations of aqueous Cr(VI), Cr(III), Fe^{3+}, Fe^{2+}, and PS were measured by using a UV-Vis spectrophotometer (Yoke UV1901, China), respectively. The concentrations of total Cr (Cr_{total}) and total Fe (Fe_{total}) in solution were determined using a Z-2000 polarized Zeeman atomic absorption spectrometer (Hitachi, Japan), respectively. The concentration of TCH in solution was measured at 280 nm using a high-performance liquid chromatograph (HPLC, C18, China).

Results and discussion

Characterizations of nZVI, nZVI-Cu, and nZVI-Cu/PS

The surface morphology and structure of nZVI, nZVI-Cu, and nZVI-Cu/PS were characterized by SEM and TEM. The results are shown in Fig. 1a–f. As seen in Fig. 1a, because the nZVI particles have magnetic properties, small particle sizes, and large specific surface areas, the particles adhere to each other to form a long chain, and the individual nZVI particles have a spherical shape. The original nZVI surface is smooth and flat with few particles on it. It can be seen from Fig. 1b that Fe^0 is in the form of granulated fuzzy particles, and a small amount of Cu is in the form of vertical strips. The surface of the nZVI-Cu bimetallic particles is rough and has more particles and rich voids, and the particles are more uniformly dispersed. As seen from Fig. 1d and e, the particles of nZVI and nZVI-Cu have a spherical structure, and the nZVI-Cu particles are loosely agglomerated. This phenomenon indicates that loading Cu on nZVI does not change the structure of nZVI, but the surface is uneven and the voids increase, which are beneficial for increasing the specific surface area of the material and achieving good adsorption and catalysis. After the activation reaction of nZVI-Cu to PS (Fig. 1c), the nZVI-Cu particles become larger with more agglomerate distribution and interparticle voids. The particles are in the form of random sheets, which may be caused by oxidation of the surface during the reaction, and corroded fragments are deposited on the surface of the particles. As shown in Fig. 1f, the edges of the nanometal particles of nZVI-Cu/PS are dispersed. This is because PS oxidizes Cu^0 of nZVI-Cu particles to form firstly an oxide shell of Cu on the surface of the particles, then oxide shell of Cu is reduced by nZVI to generate Cu^0 and Fe oxide shell, but the core is still a spherical structure of nZVI.

X-ray diffraction patterns of nZVI, nZVI-activated PS (nZVI/PS), and nZVI-Cu/PS are presented in Fig. 2. The peak at $2\theta = 44.9°$ for Fe diffraction appears, which corresponds to the diffraction of the 110 plane of body-centered cubic α-Fe^0. Although the diffraction peak appeared, the peak shape was diffuse, which confirmed that the nZVI particles synthesized by the liquid phase method are mainly in a microcrystalline state. The characteristic peak also appears in the XRD patterns of the nZVI/PS and nZVI-Cu/PS composites. This indicates that the addition of PS and Cu^{2+} did not affect the structure of nZVI, but the nZVI diffraction peak was small. This phenomenon may be because PS causes some Cu^0 and Fe^0 to be oxidized, so the nZVI in the composite may be below the detection limit of XRD.

To further analyze the surface composition and valence state of the composite system, Fig. 3 presents the XPS spectra of the nZVI and nZVI-Cu/PS composites. Figure 3a shows that nZVI and nZVI-Cu/PS exhibit two peaks at 713.3 eV and 726.2 eV, corresponding to the binding energies of Fe $2p_{1/2}$ and Fe $2p_{3/2}$, respectively. The narrow spectrum of Fe 2p is shown in Fig. 3b, and only the weak Fe^0 (706.2 eV) characteristic peak is detected. This result indicates that the nZVI surface is oxidized, which is consistent with the previous XRD characterization. Figure 3a shows the strong O 1 s signal in the spectrum of nZVI-Cu/PS. The surface of the nZVI particles is oxidized by PS to form a metal oxide, probably due to the addition of PS in nZVI-Cu. Figure 3a also shows the detection of the Cu 2p signal in the composite system. Figure 3a shows that Cu is successfully loaded onto the nZVI surface. The XPS spectrum of Cu 2p is shown in Fig. 3c. The characteristic peaks at approximately 934.5 eV and 964.3 eV correspond to the binding energy of the Cu $2p_{3/2}$ region, and the Cu $2p_{1/2}$ region includes two characteristic peaks at 943.5 eV and 955.3 eV. The characteristic peak for Cu $2p_{3/2}$ is composed of Cu^0 (934.5 eV) and $Cu(OH)_2$ (936.5 eV). The characteristic peak for Cu $2p_{1/2}$ also confirms that Cu is loaded on the nZVI surface (Pullin et al. 2017).

Single removal of Cr(VI) and TCH in different treatment systems

The removal of Cr(VI) is presented in Fig. 4a in different treatment systems. The removal efficiency of Cr(VI) is

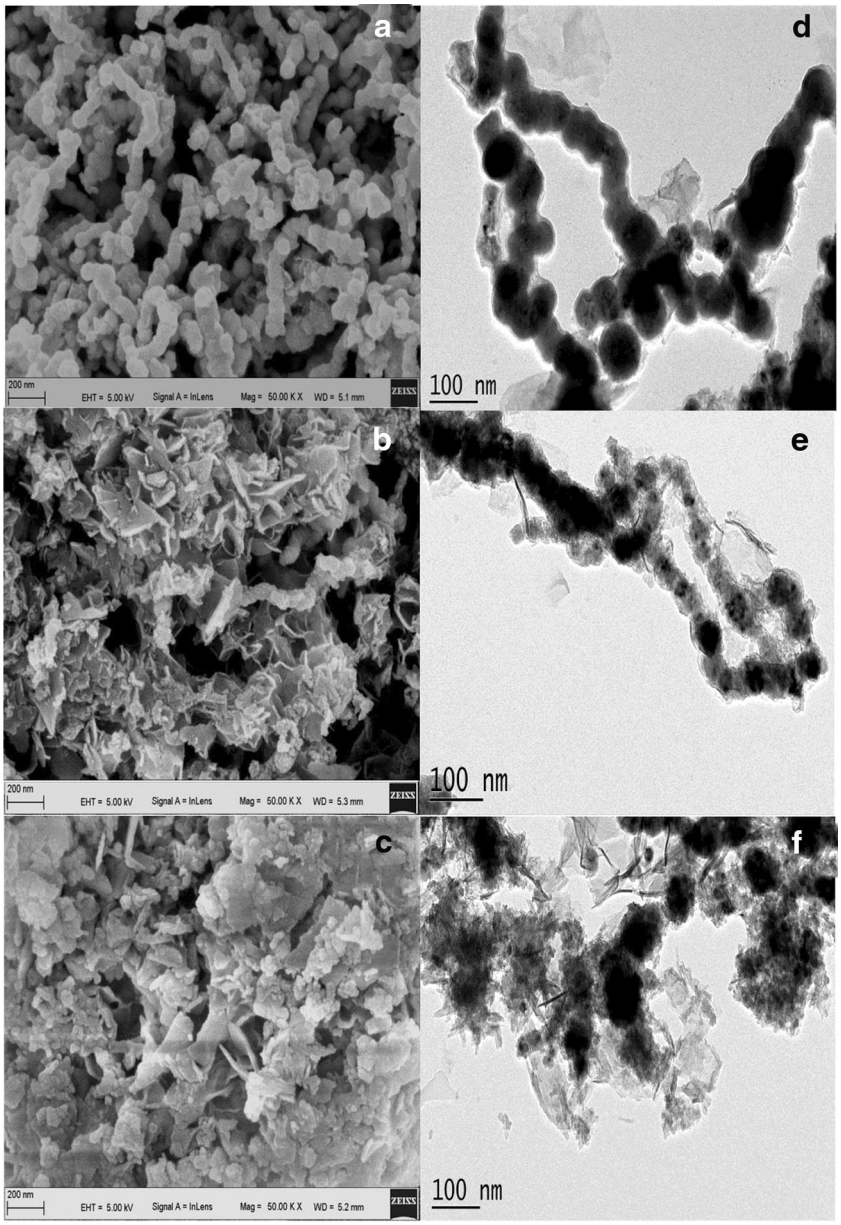

Fig. 1 FESEM images of (**a**) bare nZVI, (**b**) nZVI-Cu, and (**c**) nZVI-Cu/PS and TEM images of (**d**) bare nZVI, (**e**) nZVI-Cu, and (**f**) nZVI-Cu/PS

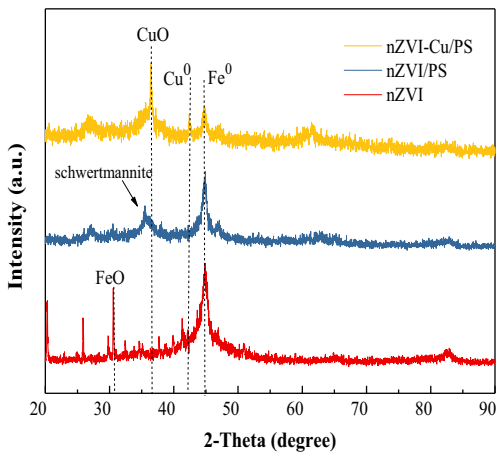

Fig. 2 XRD patterns of nZVI, nZVI/PS, and nZVI-Cu/PS

23.55%, 13.75%, 37.57%, and 55.59% after 60 min of reaction in the nZVI, PS, nZVI/PS, and nZVI-Cu systems, respectively, which is less than the removal efficiency (65.59%) of Cr(VI) in the nZVI-Cu/PS system. It is obvious that Cu significantly improved the effects of nZVI on Cr(VI) reduction due to Cu covering the surface of nZVI to form a nanoscale bimetallic layer. In addition, the presence of PS may accelerate the surface corrosion of nZVI, which exposes more reaction sites on the nZVI-Cu bimetallic surface to promote the reduction reaction between nZVI and Cr(VI). Similarly, as shown in Fig. 4b, the removal efficiency of TCH is also highest in the nZVI-Cu/PS system. On the one hand, PS is activated by Fe^{2+} and may generate some oxidative free radicals. On the other hand, a small amount of Cu transition ions may be formed on the surface of the

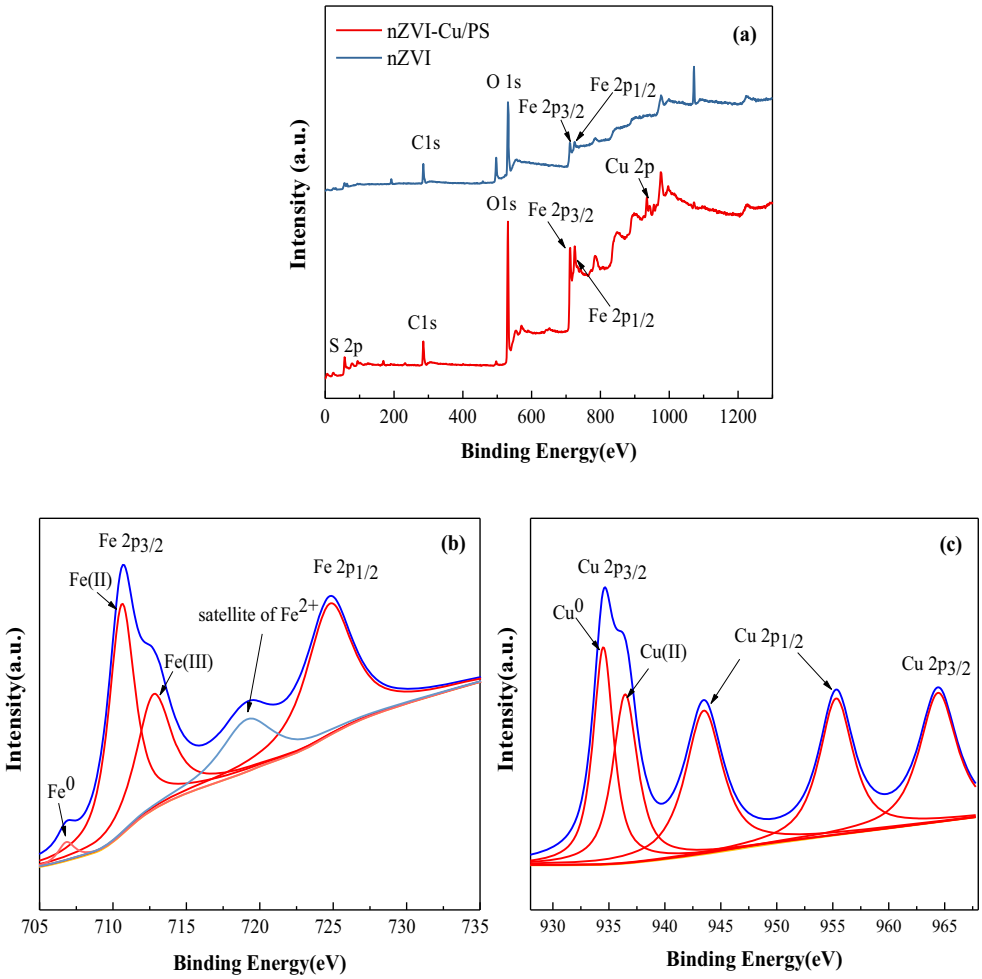

Fig. 3 Full survey XPS spectra of (**a**) nZVI and nZVI-Cu/PS, (**b**) XPS spectra of the Fe 2p region, and (**c**) XPS spectra of the Cu 2p region

bimetallic layer, which may also act as an activator of PS to degrade TCH (Deng et al. 2019; Zhou et al. 2018).

As mentioned above, depositing Cu^0 onto the surface of nZVI forms the nZVI-Cu bimetal core-shell structure. Therefore, the proportion of Cu is an important parameter for the Cr(VI) and TCH removal in the nZVI-Cu/PS system. The effects of the amount of Cu on nZVI on Cr(VI) and TCH removal are shown in Fig. 5. Figure 5a indicates that the Cr(VI) removal is rapid at the first 30 min, and then slows down. As the amount of Cu loaded on nZVI increased from 0 to 7 wt%, the removal efficiency of Cr(VI) first increased and then decreased. When the loaded amount of Cu is 3 wt%, the removal efficiency of Cr(VI) is almost 100.0% after 30 min in the nZVI-Cu/PS system. The removal efficiency of Cr(VI) decreases when the loaded amount of Cu is more than 3 wt%, but it still reaches 95.0% after 40 min. The removal

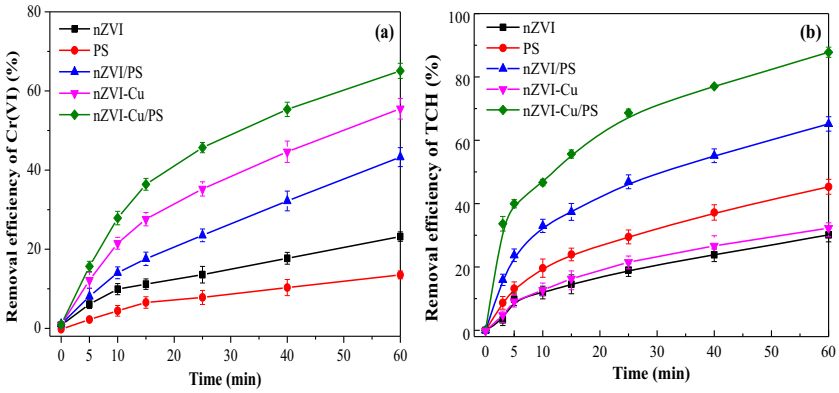

Fig. 4 The removal of Cr(VI) or TCH in the nZVI, PS, nZVI/PS, nZVI-Cu, and nZVI-Cu/PS systems

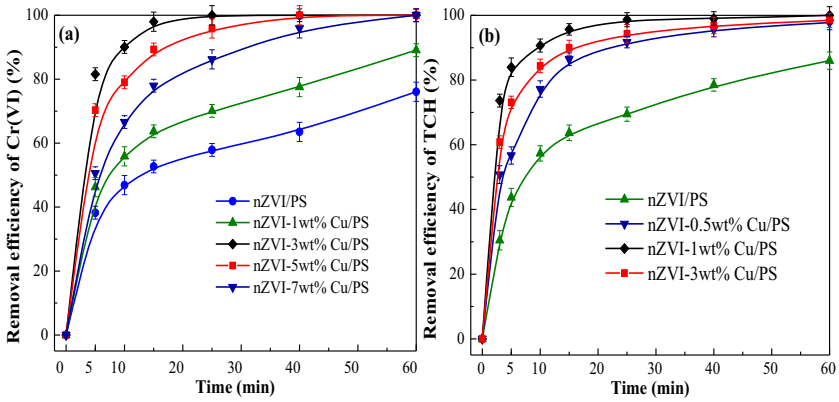

Fig. 5 Effects of amount of Cu on single pollutant removal in the nZVI-Cu/PS system

efficiency of TCH has a similar trend as Cr(VI) removal with different Cu amounts (Fig. 5b). However, the best removal effect of TCH appears when the loaded amount of Cu on nZVI is 1 wt%. Increasing the level of Cu loading provides more galvanic cells to accelerate the electron transfer, resulting in accelerated Cr(VI) and TCH removal. However, excessive Cu may also hinder and inhibit the corrosion of nZVI. Additionally, the results show that the requirements for the loaded amount of Cu on nZVI are also different for different pollutants to achieve higher removal efficiency.

Simultaneous removal of Cr(VI) and TCH in different treatment systems

From the previous experiments, it can be found that the removal efficiencies of Cr(VI) and TCH are above 95.0% when the Cu amount on nZVI is 3.0 wt%. Therefore, we used nZVI-Cu/PS loaded with 3 wt% Cu to simultaneously remove Cr(VI) and TCH, and the results are shown in Fig. 6. The PS alone has little effect on Cr(VI) removal. In the nZVI/PS system, the removal efficiencies of Cr(VI) and TCH are 44.17% and 65.39%, respectively, while the removal efficiencies of Cr(VI) and TCH are 69.01% and 80.88% in the nZVI-Cu/PS system, respectively. As described in the structural analysis of the nZVI-Cu bimetallic composite, nanoscale Cu modified the nZVI particles to enhance the reactivity of the nanoparticles and form nanobimetallics. The close and effective contact of the two nanometals enhances the transformation of electrons between them, thereby promoting the reduction of Cr(VI) in solution (Xu et al. 2012). nZVI is oxidized to form Fe^{2+}, which can activate PS and rapidly produces strong oxidizing free radicals to degrade TCH. In addition to the nZVI, Zhou et al. (2018) thought that transition ions of Cu may also acts as a new metal active site to activate PS.

Based on the above analysis, it can be concluded that the ratio of nZVI-Cu and PS may affect the removal efficiency of Cr(VI) and TCH. As shown in Fig. 7, when the proportion of nZVI-Cu increases from 1:1 to 7:1 in the nZVI-Cu/PS system, the removal efficiency of Cr(VI) and TCH increases from 61.43 and 70.53% to almost 100.0% after 40 min. However, when the dosage of

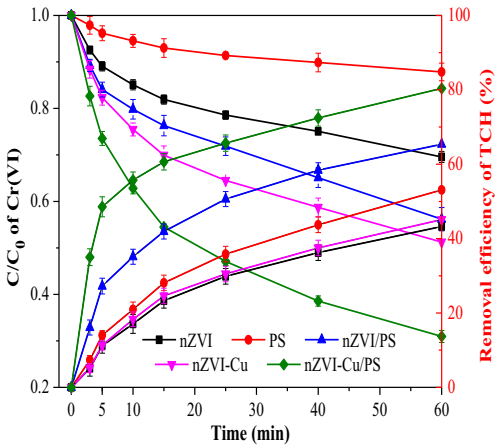

Fig. 6 Simultaneous removal of Cr(VI) and TCH in different treatment systems (ratio of nZVI-Cu and PS of 1:1)

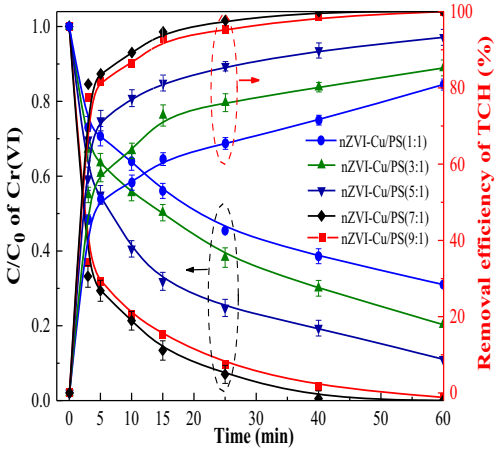

Fig. 7 Effects of different ratios of nZVI-Cu and PS on Cr(VI) and TCH removal in the nZVI-Cu/PS system

nZVI-Cu further increases, the removal efficiency of the two contaminants decreases. This is because the addition of excess nZVI-Cu leads to the rapid release of Fe^{2+}, and excess Fe^{2+} consumes free radicals in the system, which may inhibit removal of the contaminants (Li et al. 2019).

The pH is an important parameter for the treatment of wastewater. The pH value directly affects the removal ability of a treatment system for pollutants. The effects of pH on Cr(VI) and TCH removal in the nZVI-Cu/PS system are shown in Fig. 8. The removal efficiency of Cr(VI) and TCH decreases with increasing pH. Under acidic conditions, the removal efficiency of Cr(VI) and TCH is nearly 100.0% after 40 min. However, when the initial pH value of the solution is 9.0, the removal efficiency of Cr(VI) and TCH decreases to 62.17% and 66.32% after 60 min, respectively. Acidic conditions may accelerate the corrosion of nZVI-Cu to release more Fe^{2+} (Lai et al. 2013) and generate additional $SO^{-}_{4}\cdot$ (Eq. (3)–(4)). The formation of $SO^{-}_{4}\cdot$ promotes TCH degradation (Hussain et al. 2016).

$$S_2O_8^{2-} + H^+ \rightarrow HS_2O_8^- \quad (3)$$

$$HS_2O_8^- \rightarrow 2SO_4^- \cdot + H^+ \quad (4)$$

In addition, Cr(VI) is mainly present in the form of $HCrO_4^-$ under acidic conditions. While the existence of H^+ is favorable to the reduction of $HCrO_4^-$ (Eqs. (5)–(6)), acidic conditions can also effectively inhibit the deposition of precipitates on the surface of the material and allow full exposure of the active reaction sites on the nZVI-Cu surface, promoting the reduction of Cr(VI) (Qu et al. 2017).

$$HCrO_4^- + nZVI\text{–}Cu + 8H^+ \rightarrow Cu^{2+} + Fe^{2+} + Cr^{3+} + 4H_2O \quad (5)$$

$$HCrO_4^- + 3Fe^{2+} + 7H^+ \rightarrow 3Fe^{3+} + Cr^{3+} + 4H_2O \quad (6)$$

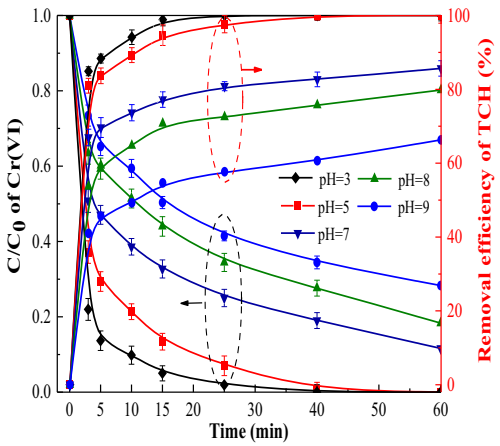

Fig. 8 Effects of pH value on the removal of Cr(VI) and TCH in the nZVI-Cu/PS system

Mechanisms of simultaneous removal of Cr(VI) and TCH

Figure 9 shows the variation in PS and different forms of Fe and Cr in solution with reaction time for nZVI-Cu/PS system. As shown in Fig. 9a, PS decreases rapidly with the reaction time, while the concentrations of Fe_{total} and Fe^{3+} in solution always increases due to the production of Fe^{3+}. Fe^{2+} is mainly derived from uncovered nZVI, and Cu^0 of the nZVI-Cu composites react with PS and Cr(VI) in the nZVI-Cu/PS system (Eqs. (7)–(10) and Eq. (2)). The concentration of Fe^{2+} increases to 0.14 mg L^{-1} (the highest value) in solution during the first 10 min and then decreases, finally maintaining a relatively stable value. Once Fe^{2+} is dissolved from the solid surface, it will react with Cr(VI) or PS. In addition, a passivation reaction of the oxide or precipitate on the nZVI surface may occur after 10 min, resulting in a slight decrease in Fe^{2+} in solution. Figure 9b indicates that the Cr(VI) and Cr_{total} concentrations decrease with the reaction time, while the concentration of Cr(III) reaches a maximum at 5 min (5.62 mg L^{-1}) and then slowly decreases at a later time. Due to the adsorption-reduction effects of nZVI-Cu on heavy metal ions in the nZVI-Cu/PS system, a large amount of Cr(VI) is reduced to Cr(III) in solution. The decrease in Cr_{total} and Cr(III) indicates that different types of Cr may be adsorbed on the solid surface of the nZVI-Cu layer.

$$nZVI\ \left(\text{uncovered by } Cu^0\right) + S_2O_8^{2-} \rightarrow Fe^{2+} + 2SO_4^{2-}. \quad (7)$$

$$Cu^0 + 1/2S_2O_8^{2-} \rightarrow Cu^+ + SO_4^{2-} \quad (8)$$

$$Cu^+ + S_2O_8^{2-} \rightarrow Cu^{2+} + SO_4^{2-} \cdot + SO_4^{2-} \quad (9)$$

$$3Cu^0 + 2Cr^{6+} \rightarrow 2Cr^{3+} + 3Cu^{2+} \quad (10)$$

The XPS spectra were also used to analyze the main elemental composition and valence states of Fe, Cu, and Cr before and after the reaction. As presented in Fig. 10a, a new characteristic peak appears near 580 eV after the reaction, and the characteristic peak belongs to the region of Cr 2p, which further confirms that Cr is adsorbed on the nZVI-Cu nanomaterial surface. Figure 10b is an XPS spectrum of the Cr 2p region; the peak at 587.3 eV in the Cr $2p_{1/2}$ region is the Cr(III) characteristic peak (Kong et al. 2016). There are three characteristic peaks in the Cr $2p_{3/2}$ region, which represent Cr(III) and Cr(VI), respectively, and the peak at 578.8 eV is indicative of $K_2Cr_2O_7$ (Paparazzo 1987; Huang et al. 2013; Liu et al. 2016). The presence of $K_2Cr_2O_7$ implies that Cr(VI) exists on the surface of the nZVI-Cu nanometal materials, and the adsorption of Cr(III) on the surface of the nanomaterials indicates that Cr(VI) is reduced during the reaction (Hu et al.

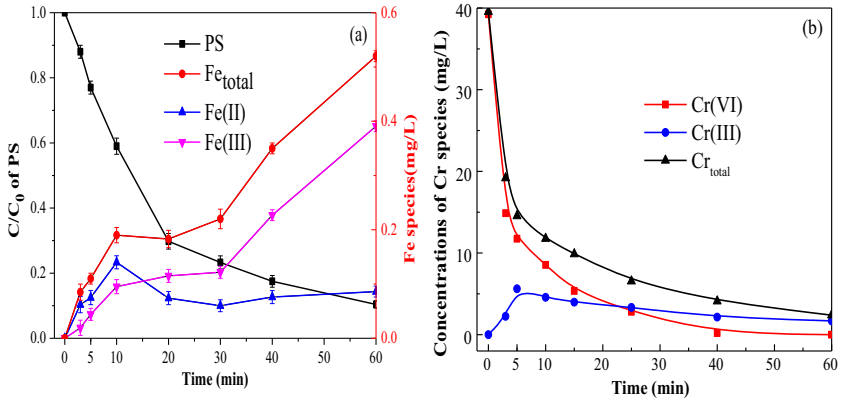

Fig. 9 The variation in PS and different forms of Fe and Cr in solution with reaction time for nZVI-Cu/PS system

2010). The results show that the nanobimetallic material achieves adsorption and reduction of Cr(VI) in the nZVI-Cu/PS system. Cr(VI) is first adsorbed on the surface by the nZVI-Cu composite, and then Cr(VI) is rapidly reduced to Cr(III) by the highly reductive nature of Cu^0. Figure 10a shows that the characteristic peaks at the Fe 2p region include the Fe 2p3/2 (713.3 eV) and the Fe 2p1/2 (726.2 eV), which are the same as before the reaction, indicating that the mixed-valence iron oxide appeared on the surface of the composite after the reaction; the characteristic peaks at Fe 2p3/2 refer to Fe^{3+} and Fe^{2+}. As shown in Fig. 10a, the Cu 2p3/2 region includes characteristic peaks of Cu 2p3/2 and Cu 2p1/2, indicating the presence of Cu^0 and Cu(II) on the surface of the composite. It can also be seen from Fig. 10 that the adsorbed Cr(VI) is reduced to Cr(III) by Cu^0 on nZVI-Cu surface (Eq. (10)), while nZVI is oxidized by Cu^{2+} to form Fe^{2+} (Eq. (2)). The generated Fe^{2+} can react with Cr(VI) to form Fe^{3+} and Cr(III) (Eq. (11)). In addition, the nZVI-Cu bimetallic materials can promote the formation of galvanic cells and enhance the electron transfer between them. A small amount of a Cu^0 layer is also formed on the surface of the nZVI-Cu composite to promote the reduction of solution Cr(VI) (Fig. 11). Since the redox potential of Cu^0 is lower than that of Cr(VI) (Hu et al. 2010), Cr(VI) undergoes a redox reaction with Cu^0 to form Cu(II) and Cr(III) (Eq. (10))

$$3Fe^{2+} + Cr^{6+} \rightarrow 3Fe^{3+} + Cr^{3+} \quad (11)$$

The removal of TCH is another important function in the nZVI-Cu/PS system (Fig. 11). The PS activated by nZVI mainly generates oxidative free radicals (such as $SO_4^{-}\cdot$ and ·OH) to degrade organic pollutants (Eqs. (12)–(14)) (Zhao et al. 2010; Yuan et al. 2014; Liu et al. 2017). In order to identify the active species which plays a predominant role to TCH degradation in the nZVI-Cu/PS system, quenching experiments were carried out, and the inhibition of TCH degradation in the presence of radical scavengers was analyzed. Based on different reaction rates, TBA and MA were used to evaluate the relative contribution of ·OH and $SO_4^{-}\cdot$ in the degradation process of TCH, and the results are shown in Fig. 12. After the addition of two capture agents, the removal efficiency of Cr(VI) hardly changes. However, the removal efficiency of TCH decreases significantly, especially when TBA is added to the reaction system.

$$Fe^{2+} + S_2O_8^{2-} \rightarrow SO_4^{-}\cdot + SO_4^{2-} + Fe^{3+} \quad (12)$$

$$SO_4^{-}\cdot + H_2O \rightarrow \cdot OH + H^+ + SO_4^{2-} \quad (13)$$

$$SO_4^{-}\cdot + OH^- \rightarrow \cdot OH + SO_4^{2-} \quad (14)$$

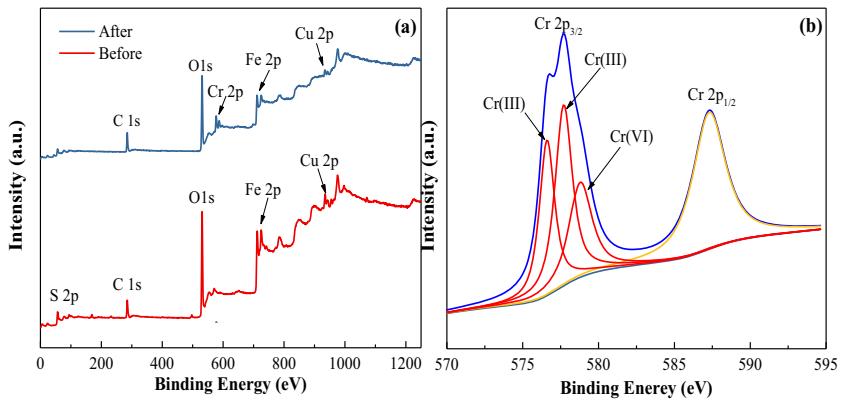

Fig. 10 **a** XPS spectra of nZVI-Cu/PS before and after the reaction. **b** XPS spectra of the Cr 2p region after the reaction

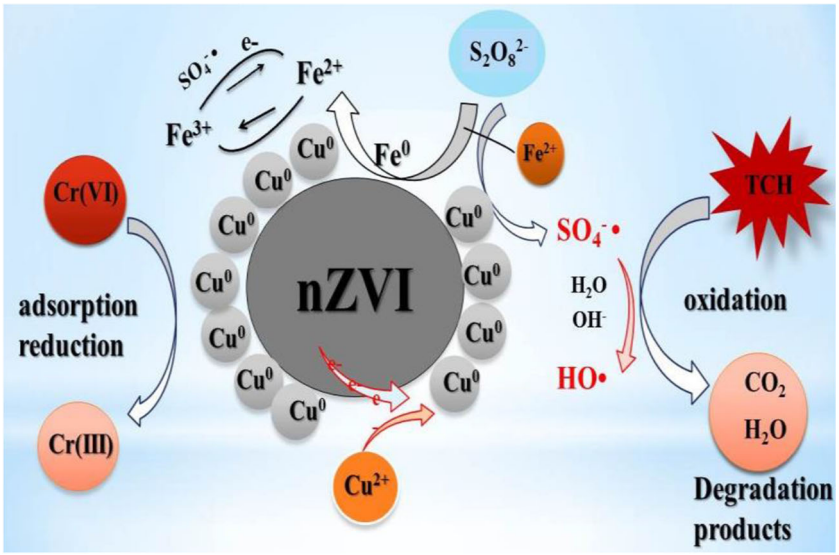

Fig. 11 Mechanisms of simultaneous removal of Cr(VI) and TCH in the nZVI-Cu/PS system

According to previous reports, the relative contributions of $SO_4^{-}\cdot$ and ·OH can be determined by analyzing the difference in the rate constant of the pollutant removal with different scavengers (Ahmad et al. 2012; Oh et al. 2016). As shown in Table 1, the pseudo-first order rate constants of TCH degradation without a scavenger and with TBA are 0.1287 and 0.0779 min^{-1} in the nZVI-Cu/PS system, respectively. The relative contribution of ·OH can be estimated to be 39.5%. However, the addition of MA further increases the inhibition; the rate constant decreases to 0.0151 min^{-1}. The difference between inhibition caused by TBA and MA can be attributed to the function of $SO_4^{-}\cdot$. Thus, the relative contribution of $SO_4^{-}\cdot$ is estimated to be 48.8%. This suggests that $SO_4^{-}\cdot$ plays a predominant role in TCH degradation, which is consistent with other literature (Kim et al. 2018). It is also indicated that the involvement of free radicals that have not been identified because the sum of contributions of $SO_4^{-}\cdot$ and ·OH is less than 100%.

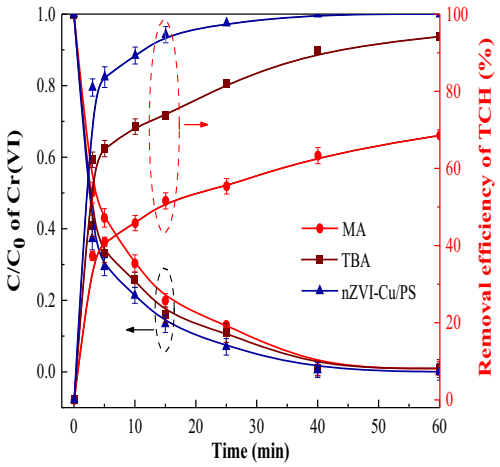

Fig. 12 Effects of TBA and MA on Cr(VI) and TCH removal in the nZVI-Cu/PS system

Conclusion

This study has demonstrated for the first time that nZVI-Cu/PS can simultaneously remove Cr(VI) and TCH from aqueous solutions. Compared with PS, nZVI nZVI/PS, and nZVI-Cu, nZVI-Cu/PS exhibited faster and more effective reduction of Cr(VI) and oxidation of TCH. Nanoscale Cu covers the surface of the nZVI to form a nanobimetallic and significantly improved the effect of nZVI on Cr(VI) reduction. The loaded amount of Cu on nZVI and the ratio of nZVI-Cu and PS affected the removal efficiency of Cr(VI) and TCH. Acidic conditions are more favorable for the activation of PS and the corrosion of nZVI than alkaline conditions. The $SO_4^{-}\cdot$ produced from PS activated by the nZVI-Cu nanobimetallic is identified as the main active oxygen species responsible for TCH degradation, and the activation process is in a continuous state.

Table 1 Change in the kinetic constant, k, for Cr(VI) and TCH removal after adding different radical scavengers to the nZVI-Cu/PS system

Contaminant	Pseudo-first order kinetic constant k (min^{-1})		
	MA	TBA	Without
TCH	0.0151	0.0779	0.1287
Cr(VI)	0.1008	0.1045	0.1163

References

Ahmad M, Teel AL, Furman OS, Reed JI, Watts RJ (2012) Oxidative and reductive pathways in iron-ethylenediaminetetraacetic acid-activated persulfate systems. J Environ Eng 138:411–418

Chen WS, Su YC (2012) Removal of dinitrotoluenes in wastewater by sono-activated persulfate. Ultrason Sonochem 19:921–927

Criquet J, Leitner NKV (2011) Electron beam irradiation of aqueous solution of persulfate ions. Chem Eng J 169:258–262

Deng J, Xu MY, Chen YJ, Li J, Qiu CE, Li XY, Zhou SQ (2019) Highly-efficient removal of norfloxacin with nanoscale zero-valent copper activated persulfate at mild temperature. Chem Eng J 366:491–503

Diao ZH, Xu XR, Chen H, Jiang D, Yang YX, Kong LJ, Sun YX, Hu YX, Hao QW, Liu L (2016) Simultaneous removal of Cr(VI) and phenol by persulfate activated with bentonite-supported nanoscale zero-valent iron: reactivity and mechanism. J Hazard Mater 316: 186–193

Ghauch A, Ayoub G, Naim S (2013) Degradation of sulfamethoxazole by persulfate assisted micrometric Fe-0 in aqueous solution. Chem Eng J 228:1168–1181

Guo XJ, Yang Z, Dong HY, Guan XH, Ren QD, Lv XF, Jin X (2016) Simple combination of oxidants with zero-valent-iron (ZVI) achieved very rapid and highly efficient removal of heavy metals from water. Water Res 88:671–680

Hosseini SM, Ataie-Ashtiani B, Kholghi M (2011) Nitrate reduction by nano-Fe/Cu particles in packed column. Desalination 276:214–221

Hu CY, Lo SL, Liou YH, Hsu YW, Shih KM, Lin CJ (2010) Hexavalent chromium removal from near natural water by copper-iron bimetallic particles. Water Res 44:3101–3108

Huang PP, Ye ZF, Xie WM, Chen Q, Li J, Xu ZC, Yao MS (2013) Rapid magnetic removal of aqueous heavy metals and their relevant mechanisms using nanoscale zero valent iron (nZVI) particles. Water Res 47:4050–4058

Hussain I, Li MY, Zhang YQ, Li YC, Huang SB, Du XD, Liu GQ, Hayat W, Anwar N (2016) Insights into the mechanism of persulfate activation with nZVI/BC nanocomposite for the degradation of nonylphenol. Chem Eng J 311:163–172

Kang YG, Yoon H, Lee W, Kim EJ, Chang YS (2018) Comparative study of peroxide oxidants activated by nZVI: removal of 1,4-Dioxane and arsenic(III) in contaminated waters. Chem Eng J 334: 2511–2519

Kim C, Ahn JY, Kim TY, Shin WS, Hwang I (2018) Activation of persulfate by nanosized zero-valent iron (nZVI): mechanisms and transformation products of nZVI. Environ Sci Technol 52:3625–3633

Kong XK, Han ZT, Zhang W, Song L, Li H (2016) Synthesis of zeolite-supported microscale zero-valent iron for the removal of Cr^{6+} and Cd^{2+} from aqueous solution. J Environ Manag 169:84–90

Lai B, Chen ZY, ZhouYX YP, Wang JL, Chen ZQ (2013) Removal of high concentration p-nitrophenol in aqueous solution by zero valent iron with ultrasonic irradiation (US-ZVI). J Hazard Mater 250–251: 220–228

Li M, Yang XF, Wang DS, Yuan J (2017) Enhanced oxidation of erythromycin by persulfate activated iron powder-H_2O_2 system: role of the surface Fe species and synergistic effect of hydroxyl and sulfate radicals. Chem Eng J 317:103–111

Li Y, Han DH, Arai YJ, Fu X, Li XQ, Huang WL (2019) Kinetics and mechanisms of debromination of tetrabromobisphenol A by Cu coated nano zerovalent iron. Chem Eng J 373:95–103

Lin YT, Liang CJ, Chen JH (2011) Feasibility study of ultraviolet activated persulfate oxidation of phenol. Chemosphere 82:1168–1172

Liu Q, Xu MJ, Li F, Wu T, Li YJ (2016) Rapid and effective removal of Cr(VI) from aqueous solutions using the $FeCl_3/NaBH_4$ system. Chem Eng J 296:340–348

Liu YD, Zhou AG, Gan YQ, Li XQ (2017) Roles of hydroxyl and sulfate radicals in degradation of trichloroethene by persulfate activated with Fe^{2+} and zero-valent iron: insights from carbon isotope fractionation. J Hazard Mater 344:98–103

Matzek LW, Carter KE (2016) Activated persulfate for organic chemical degradation: a review. Chemosphere 151:178–188

Oh WD, Dong ZL, Lim TT (2016) Generation of sulfate radical through heterogeneous catalysis for organic contaminants removal: current development challenges and prospects. Appl Catal B Environ 194: 169–201

Paparazzo E (1987) XPS and auger spectroscopy studies on mixtures of the oxides SiO_2, Al_2O_3, Fe_2O_3, and Cr_2O_3. J Electron Spectrosc 43: 97–112

Pullin H, Crane RA, Morgan DJ, Scott TB (2017) The effect of common groundwater anions on the aqueous corrosion of zero-valent iron nanoparticles and associated removal of aqueous copper and zinc. J Environ Chem Eng 5:1166–1173

Qu GZ, Kou LQ, Wang TC, Liang DL, Hu SB (2017) Evaluation of activated carbon fiber supported nanoscale zero-valent iron for chromium (VI) removal from groundwater in a permeable reactive column. J Environ Manag 201:378–387

Qu GZ, Zeng DY, Chu RJ, Wang TC, Liang DL, Qiang H (2019) Magnetic Fe_3O_4 assembled on nZVI supported on activated carbon fiber for Cr(VI) and Cu(II) removal from aqueous solution through a permeable reactive column. Environ Sci Pollut Res 26:5176–5188

Sheng GD, Shao XY, Li YM, Li JF, Dong HP, Cheng W, Gao X, Huang YY (2014) Enhanced removal of U(VI) by nanoscale zerovalent iron supported on Na-bentonite and an investigation of mechanism. J Phys Chem A 118:2952–2958

Sheng GD, Hu J, Li H, Li JX, Huang YY (2016) Enhanced sequestration of Cr(VI) by nanoscale zero-valent iron supported on layered double hydroxide by batch and XAFS study. Chemosphere 148:227–232

Shi JL, Long C, Li AM (2016) Selective reduction of nitrate into nitrogen using Fe-Pd bimetallic nanoparticle supported on chelating resin at near-neutral pH. Chem Eng J 286:408–415

Song QY, Feng YP, Liu GG, Lv WY (2019) Degradation of the flame retardant triphenyl phosphate by ferrous ion-activated hydrogen peroxide and persulfate: kinetics, pathways, and mechanisms. Chem Eng J 361:929–936

Waldemer RH, Tratnyek PG, Johnson RL, Nurmi JT (2007) Oxidation of chlorinated ethenes by heat-activated persulfate: kinetics and products. Environ Sci Technol 41:1010–1015

Wei JJ, Xu XH, Liu Y, Wang DH (2006) Catalytic hydrodechlorination of 2,4-dichlorophenol over nanoscale Pd/Fe: reaction pathway and some experimental parameters. Water Res 40:348–354

Xu XR, Li XZ (2012) Degradation of azo dye Orange G in aqueous solutions by persulfate with ferrous ion. Sep Purif Technol 72: 105–111

Xu FY, Deng SB, Xu J, Zhang W, Wu M, Wang B, Huang J, Yu G (2012) Highly active and stable Ni-Fe bimetal prepared by ball milling for catalytic hydrodechlorination of 4-chlorophenol. Environ Sci Technol 46:4576–4582

Yuan SH, Liao P, Alshawabkeh AN (2014) Electrolytic manipulation of persulfate reactivity by iron electrodes for trichloroethylene degradation in groundwater. Environ Sci Technol 48:4632–4633

Zeng YB, Walker H, Zhu QZ (2017) Reduction of nitrate by NaY zeolite supported Fe, Cu/Fe and Mn/Fe nanoparticles. J Hazard Mater 324: 605–616

Zhao JY, Zhang YB, Quan X, Chen S (2010) Enhanced oxidation of 4-chlorophenol using sulfate radicals generated from zero-valent iron and peroxydisulfate at ambient temperature. Sep Purif Technol 71: 302–307

Zhou P, Zhang J, Zhang YL, Zhang GC, Li WS, Wei CM, Liang J, Liu Y, Shu SH (2018) Degradation of 2,4-dichlorophenol by activating persulfate and peroxomonosulfate using micron or nanoscale zero-valent copper. J Hazard Mater 344:1209–1219

Zhu BW, Lim TT (2007) Catalytic reduction of chlorobenzenes with Pd/Fe nanoparticles: reactive sites, catalyst stability, particle aging, and regeneration. Environ Sci Technol 41:7523–7529